Dissolution Behavior of Ferritic Stainless Steel in Liquid Magnesium

Taninouchi, Yu-ki
Department of Materials Science & Engineering, Kyushu University

Yamaguchi, Tsubasa
Faculty of Engineering, Kyushu University

Okabe, Toru H.
Institute of Industrial Science, The University of Tokyo

Nakano, Hiroaki
Department of Materials Science & Engineering, Kyushu University

出版情報：ISIJ International. 63 (1), pp.150-158, 2023-01-15. 日本鉄鋼協会
バージョン：

ISIJ International, Vol. 63 (2023), No. 1, pp. 150–158
https://doi.org/10.2355/isijinternational.ISIJINT-2022-232

Dissolution Behavior of Ferritic Stainless Steel in Liquid Magnesium

Yu-ki TANINOUCHI,[1)*] Tsubasa YAMAGUCHI,[2)] Toru H. OKABE[3)] and Hiroaki NAKANO[1)]

1) Department of Materials Science & Engineering, Kyushu University, 744 Motooka Nishi-ku, Fukuoka, 819-0395 Japan.
2) Faculty of Engineering, Kyushu University, 744 Motooka Nishi-ku, Fukuoka, 819-0395 Japan.
3) Institute of Industrial Science, The University of Tokyo, 4-6-1 Komaba Meguro-ku, Tokyo, 153-8505 Japan.

(*Received on May 9, 2022; accepted on September 13, 2022*)

Steel containers and equipment are used to handle Mg and Mg-alloy melts in industrial processes such as Mg casting and Ti smelting. In this study, the dissolution behavior of SUS430 ferritic stainless steel in liquid Mg was quantitatively evaluated in order to obtain fundamental information on the contamination of Mg with steel materials in these industrial processes. Pure Mg was sealed in a SUS430 crucible and melted at 1 073–1 273 K for 24–96 h. In addition to Fe and Cr, some minor elements in the SUS430 (Mn, Ni, and Cu) were evaluated as impurity elements dissolved in liquid Mg. The concentrations of Fe and Cr in liquid Mg reached a steady state within 24 h, and the empirical equations describing their temperature dependence were obtained. In contrast, the concentrations of Mn, Ni, and Cu in Mg increased with increase in melt holding time. With the dissolution of these elements, a region with Mn concentration lower than that of the original composition was formed on the inner wall of the SUS430 crucible. The validity of the experimental values of impurity concentration in Mg was discussed based on the thermodynamic data of Mg–*i* (*i* = Fe, Cr, Mn, Ni, and Cu) binary systems and SUS430. Furthermore, impurity uptake through liquid Mg during Ti production using the Kroll process was preliminary discussed. The findings of this study provide important and beneficial information for improving impurity control in the melting and casting of Mg and in Ti smelting using Mg as a reductant.

KEY WORDS: stainless steel; magnesium; liquid metal; dissolution; impurity contamination.

1. Introduction

Metallic Fe does not form intermetallic compounds with Mg, and it has a low solubility limit in liquid Mg.[1,2)] Therefore, steel crucibles and equipment are commonly used for the melting and casting of Mg and its alloys.[3)] In Mg production via molten salt electrolysis, steel materials are occasionally used as cathodes for electrochemical deposition of liquid Mg.[4)] Furthermore, in Ti smelters, where the magnesiothermic reduction of $TiCl_4$ produces metallic Ti (Ti sponge), steel containers and pipes are used for the storage and transportation of liquid Mg.[4,5)]

Although the extent of Fe dissolution from steel materials into Mg and its alloy melts is relatively low, it is industrially crucial to understand and control this phenomenon. For example, Fe contamination can adversely affect the corrosion resistance of Mg and its alloys.[6,7)] In the case of Mg alloys used for structural applications, Fe concentration is typically regulated to be ≤50 mass ppm to ensure sufficient corrosion resistance. As another example, the Ti sponge produced during the Ti smelting process absorbs Fe and other impurities in liquid Mg used as a reductant.[5)] Thus, Fe and other impurities, dissolved from steel materials into liquid Mg in Ti smelters, reduce the quality and producibility of the Ti sponge.

In terms of the mechanical properties of steel, special steel materials are often used for constructing components that are exposed to Mg-based melts. In such cases, in addition to Fe, alloying and impurity elements in the steels tend to dissolve in the melts. For example, stainless steels (such as SUS430) are used as crucible materials for melting Mg.[3)] In stainless steels, Cr is added more than 10.5 mass%; it dissolves from the steels into the melt, albeit in small amounts. Ni, which is often added in special steels, has a high affinity with Mg.[8)] When liquid Mg comes in contact with special steels with high Ni content (such as austenitic stainless steels, including SUS304 and SUS316), a considerable amount of Ni dissolves from the steel surface into the melt.[7,9)] Thus, direct contact between the Mg-based melts and steel materials with high Ni content should be avoided during industrial processes. Austenitic stainless steel containers lined with carbon steel are occasionally used when

* Corresponding author: E-mail: taninouchi.yuki.329@m.kyushu-u.ac.jp

excellent mechanical properties at high temperatures are required for the steel containers.

Quantitative data about the dissolution of various steel materials in Mg and its alloy melts and about changes in the steel surfaces due to contact with the melts can provide insights for improving impurity control in industrial processes such as Mg alloy production and Ti smelting. However, the number of studies on this subject are limited,[9–20] and the details are still unclear.

Table 1 lists previous studies on the quantitative dissolution of steels in Mg-based melts.[9,16–20] For ferritic stainless steels, Kaitoh *et al.* melted high-purity Mg in a SUS430 crucible and reported the impurity concentration in the Mg.[16] The surface of the SUS430 crucible was pre-treated to form a MgO layer; after melting Mg at 973 K for 1.5 h, the concentrations of Fe and Cr in the Mg were determined to be 0.001 mass% and <0.001 mass%, respectively. Sonoda *et al.* melted a non-combustible Mg alloy (AZX912) in a SUS430 crucible and reported the impurity uptake and its effect on the corrosion resistance of the Mg alloy.[18] When the AZX912 alloy was melted at 1 003 K for 1 h, Fe concentration in the Mg alloy increased to 0.012–0.015 mass% owing to dissolution from SUS430; on the other hand, Cr contamination was not detected by inductively coupled plasma-atomic emission spectrometry (ICP-AES).

The limited quantitative data about the dissolution of various steels in Mg and its alloy melts are available. Thus, the authors focused on SUS430 ferritic stainless steel, which is used as a crucible material in the industry, and investigated the dissolution behavior of this stainless steel in liquid Mg at 1 073–1 273 K. In addition to Fe and Cr, some minor elements in the steel (Mn, Ni, and Cu) were quantitatively evaluated as impurities dissolved in Mg. The validity of the experimental data was discussed on the basis of the thermodynamic data of Mg–*i* (*i* = Fe, Cr, Mn, Ni, and Cu) binary systems and SUS430. Additionally, impurity uptake through liquid Mg in Ti smelting was preliminary discussed using the obtained experimental data.

2. Experimental

2.1. Materials

Figure 1 shows a photograph of the materials used in this study; **Table 2** presents the compositions of Mg and ferritic 430 stainless steel. Commercial Mg rods (diameter (ϕ) =

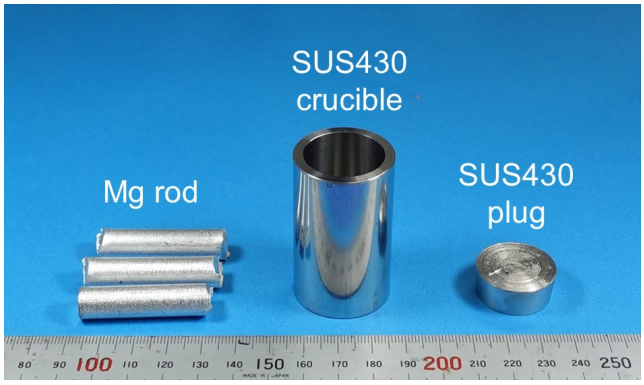

Fig. 1. Photograph of materials used in this study. (Online version in color.)

Table 1. Representative studies on the quantitative dissolution of steel materials in Mg or Mg-alloy melts.[9,16–20]

Authors, Year	Steel/Melt	Temperature	Ref.
Kaitoh *et al.*, 1995	Low carbon steel/pure Mg	973 K	16
	Ferritic stainless steel (JIS SUS430)[a]/pure Mg		
Scharf & Ditze, 2007	Low carbon steel/Mg–Al alloy	953–1 043 K	17
	Low carbon steel/AZ91[b]	1 043–1 103 K	
	Low carbon steel/AS31[c]	953–1 043 K	
Sonoda *et al.*, 2016	Ferritic stainless steel (JIS SUS430)/AZX912[d]	903–1 003 K	18
Taninouchi *et al.*, 2018	Low carbon steel/pure Mg	1 073–1 323 K	9
	Austenitic stainless steel (JIS SUS316)/pure Mg		
	Pure Fe/pure Mg		
Chen *et al.*, 2020	Low carbon steel/AZ91[b]	923–1 053 K	19
	Low carbon steel/AM50[e]		
	Chromium molybdenum steel (AISI H13)/AZ91[b]		
	Chromium molybdenum steel (AISI H13)/AM50[e]		
	Duplex stainless steel (GB 022Cr25Ni7Mo4N)/AZ91[b]		
	Duplex stainless steel (GB 022Cr25Ni7Mo4N)/AM50[e]		
Taninouchi & Okabe, 2021	Austenitic stainless steel (JIS SUS316)/Mg–Ni alloy	1 073–1 273 K	20

a: Surface treatment to form an MgO layer was conducted.
b: Commercial Mg alloy containing ~9 mass% Al and ~1 mass% Zn.
c: Commercial Mg alloy containing ~3 mass% Al and ~1 mass% Si.
d: Commercial Mg alloy containing ~9 mass% Al, ~1 mass% Zn, and 2 mass% Ca.
e: Commercial Mg alloy containing ~5 mass% Al and ~0.4 mass% Mn.

Table 2. Typical compositions of Mg and SUS430 used in this study.

	Concentration of element i, C_i (mass%)									
	Mg	Fe	Cr	Mn	Ni	Cu	Si	C	P	S
Mg	>99.9	0.009	<0.001	0.003	<0.001	<0.001	–[a]	–[a]	–[a]	–[a]
SUS430	–[a]	82[b]	16.3	0.92	0.22	0.18	0.22	0.09	0.03	0.002

a: No data.
b: $C_{Fe} = 100 - (C_{Cr} + C_{Mn} + C_{Ni} + C_{Cu} + C_{Si} + C_C + C_P + C_S)$.

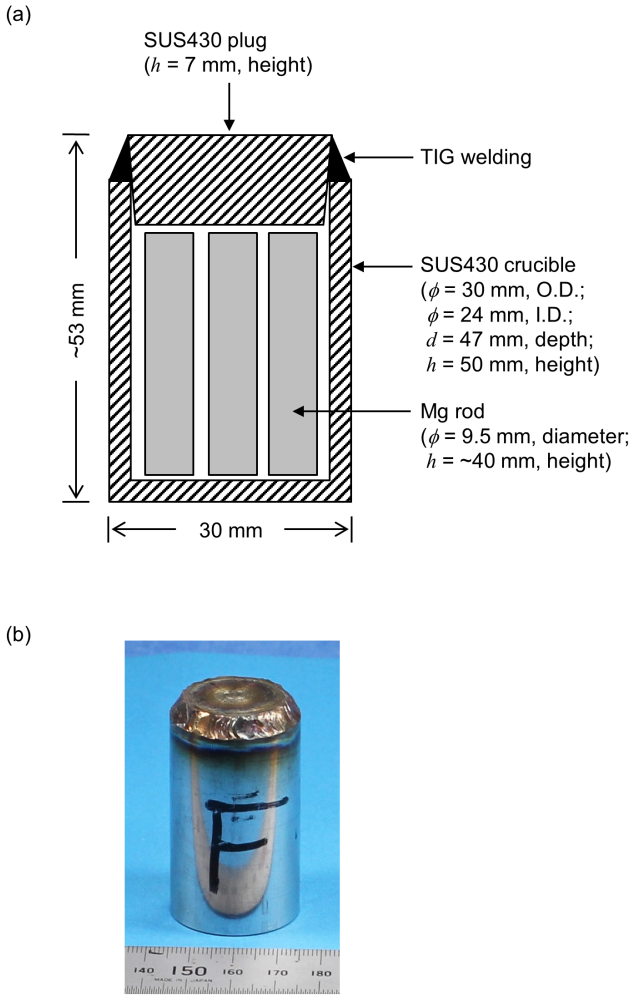

Fig. 2. (a) Schematic illustration and (b) photograph of closed crucible for holding liquid Mg (Exp. SUS430_06). (Online version in color.)

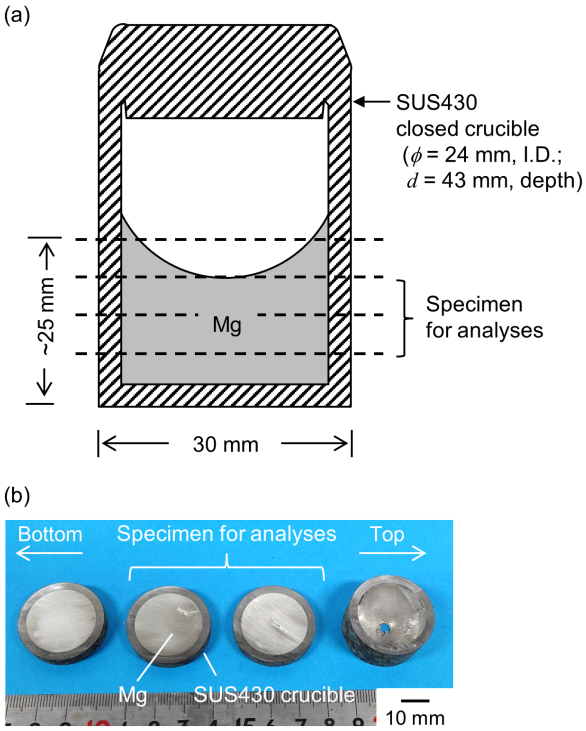

Fig. 3. (a) Schematic illustration of the closed crucible after the melt holding process. Dashed lines indicate the cut-out positions. (b) Photograph of typical specimens cut from the closed crucible (Exp. SUS430_09). (Online version in color.)

9.5 mm; Nilaco Corporation) with purity >99.9 mass% were used. Typical concentrations of impurities determined by ICP-AES were 0.009 mass% Fe, <0.001 mass% Cr, 0.003 mass% Mn, <0.001 mass% Ni, and <0.001 mass% Cu. The crucibles (outer diameter (O.D.) = 30 mm; inner diameter (I.D) = 24 mm; depth (d) = 47 mm) and plugs were fabricated by lathing a hot-finished round bar of JIS SUS430.[21] The concentration of Cr in the SUS430 was approximately 16 mass%. Additionally, typical concentrations of Mn, Ni, Cu, and Si were 0.92, 0.22, 0.18, and 0.22 mass%, respectively. The relatively large amount of Cu in the SUS430 was probably attributed to the use of scraps as some of the raw materials.

2.2. Magnesium-melt Holding Process

At high temperatures, metallic Mg is highly volatile and highly reactive with oxygen and nitrogen. Therefore, the SUS430 crucible containing the Mg rods was sealed by a plug using tungsten inert gas (TIG) welding, as shown in **Fig. 2**. The mass of Mg held in the crucible was 14.5 ± 2.0 g.

The Mg metal sealed in the SUS430 crucible was placed in an electric furnace under an Ar atmosphere and melted; the holding temperature and time were in the range of 1 073–1 273 K and 24–96 h, respectively. After reaching the prescribed holding time, the crucible was removed from the furnace and immediately quenched in water. For subsequent analyses, disk-shaped specimens were cut from the quenched crucible, as shown in **Fig. 3**.

2.3. Characterization

The composition of the melted Mg was determined by ICP-AES. An analytical sample of Mg was cut from the disk-shaped specimen (Fig. 3(b)). After polishing with SiC grinding paper and pickling with 0.2 M HCl(*aq.*), approximately 1 g of the Mg sample was dissolved in 100 mL of 6

M HCl(*aq.*). To prepare an analytical solution, the obtained solution was diluted with 6 M HCl(*aq.*) as needed. Thereafter, the concentrations of Fe, Cr, Mn, Ni, and Cu in the analytical solution were measured using an iCAP PRO XP Duo system (Thermo Fisher Scientific).

Analytical errors in the ICP-AES data were assessed based on the uncertainty of the calibration curve and repeatability of the measurements. The concentrations of Fe, Cr, and Mn in the analytical solutions were in the range of 1–10 ppm, while the corresponding analytical errors of Fe, Cr, and Mn were approximately 3, 3, and 4%, respectively. The concentrations of Ni and Cu in the analytical solutions were in the ranges of 0.4–7 ppm and 0.3–5 ppm, respectively, with analytical errors of approximately 3% each.

In a specific experiment, the composition and microstructure of the inner wall of the SUS430 crucible, which was in contact with liquid Mg, were evaluated by electron probe microanalysis (EPMA). The surfaces of the disk-shaped specimens (Fig. 3(b)) were polished using SiC grinding paper and then buffed. Subsequently, the interfaces between Mg and SUS430 were analyzed using an EPMA-1720 system (Shimadzu Corporation).

3. Results

3.1. Composition of Magnesium

Table 3 shows the composition of Mg melted in the SUS430 crucible under different conditions. The concentration of each impurity element in Mg (C_i (mass%), i = Fe, Cr, Mn, Ni, and Cu) increased owing to dissolution from SUS430. The impurities in Mg under each melt holding process condition were $C_{Fe} > C_{Cr} \approx C_{Mn} > C_{Ni} > C_{Cu}$. The value of C_i increased with an increase in the melt holding temperature at a constant holding time of liquid Mg.

Figure 4 demonstrates C_i as a function of melt holding time. The values of C_{Fe} and C_{Cr} remained constant for all melt holding temperatures over a holding time of 24–96 h. The dissolution of Fe and Cr from SUS430 ceased within 24 h. In contrast, the values of C_{Mn}, C_{Ni}, and C_{Cu} increased with an increase in the holding time. The dissolution of Mn, Ni, and Cu from SUS430 was considered to continue even after 96 h.

Figure 5 shows the dependence of C_{Fe} and C_{Cr} on the melt holding temperature. The logarithm of C_{Fe} and C_{Cr} had a linear relationship with the reciprocal of absolute temperature (T/K). The empirical equations of the steady-state concentrations of Fe and Cr in liquid Mg ($C^*_{i\text{ in Mg}}$ (mass%), i = Fe or Cr), which were determined by the least squares method, are as follows:

$$\log\left(C^*_{\text{Fe in Mg}}\right) = -3.68\times10^3 / T + 2.33(\pm0.02) \quad [1\,073-1\,273\ \text{K}], \quad \ldots (1)$$

$$\log\left(C^*_{\text{Cr in Mg}}\right) = -4.37\times10^3 / T + 2.43(\pm0.02) \quad [1\,073-1\,273\ \text{K}], \quad \ldots (2)$$

where the uncertainties in $\log(C^*_{i\text{ in Mg}})$ were evaluated by twice the standard error of linear regression.

Table 3. Chemical composition of Mg melted in the SUS430 crucible.

Exp. no.	Mass of Mg, w_{Mg}/g	Melt holding process		Conc. of element i in Mg, C_i (mass%)				
		Temp., T/K [a]	Time, t'/h	Fe	Cr	Mn	Ni	Cu
SUS430_01	14.90	1 073	24	0.0835	0.0235	0.0152	0.0043	0.0033
				(±0.0033)	(±0.0013)	(±0.0006)	(±0.0002)	(±0.0002)
SUS430_03	15.70		48	0.0822	0.0229	0.0212	0.0074	0.0056
				(±0.0034)	(±0.0012)	(±0.0008)	(±0.0003)	(±0.0003)
SUS430_06	14.40		96	0.0815	0.0223	0.0263	0.0095	0.0070
				(±0.0025)	(±0.0008)	(±0.0009)	(±0.0003)	(±0.0002)
SUS430_04	12.97	1 173	24	0.153	0.0489	0.0357	0.0106	0.0082
				(±0.005)	(±0.0013)	(±0.0013)	(±0.0004)	(±0.0003)
SUS430_07	15.28		48	0.155	0.0488	0.0423	0.0158	0.01200
				(±0.005)	(±0.0013)	(±0.0014)	(±0.0005)	(±0.0003)
SUS430_09	14.72		96	0.153	0.0486	0.0491	0.0221	0.0173
				(±0.005)	(±0.0013)	(±0.0016)	(±0.0007)	(±0.0004)
SUS430_05	12.50	1 273	24	0.284	0.100	0.0765	0.0374	0.0283
				(±0.008)	(±0.002)	(±0.0040)	(±0.0012)	(±0.0007)
SUS430_08	15.47		48	0.288	0.101	0.0858	0.0420	0.0312
				(±0.008)	(±0.002)	(±0.0045)	(±0.0013)	(±0.0007)
SUS430_10	14.84		96	0.284	0.0995	0.107	0.0658	0.0502
				(±0.008)	(±0.0023)	(±0.004)	(±0.0020)	(±0.0011)

a: Uncertainty of temperature ±5 K.

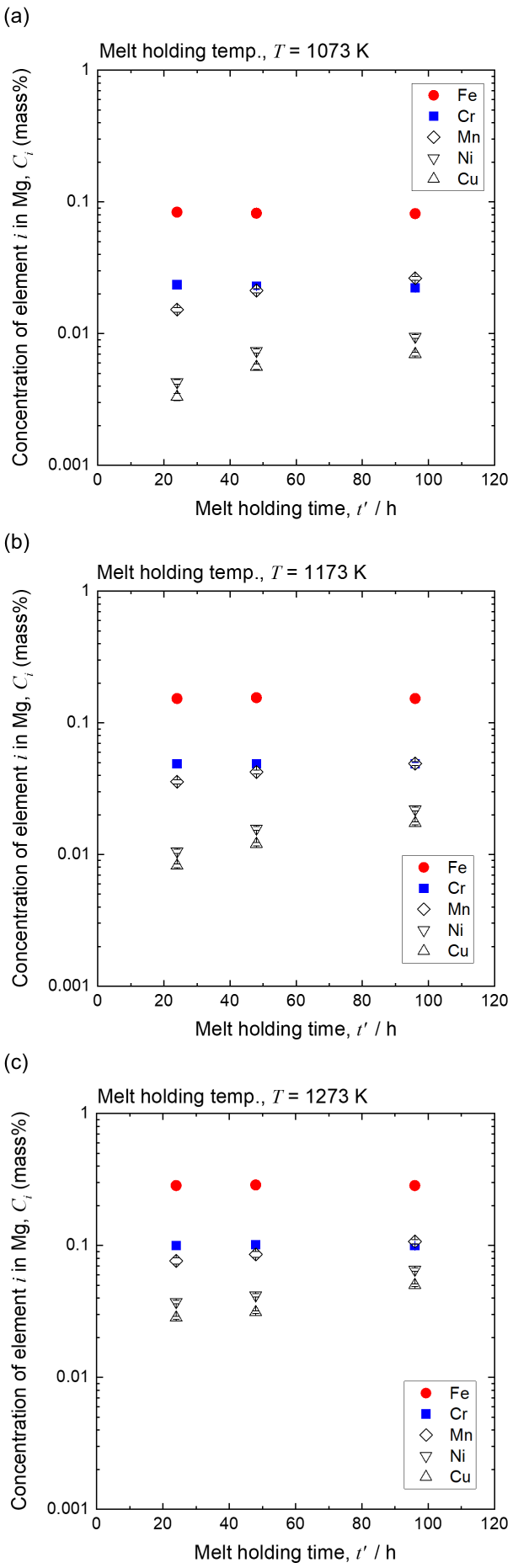

Fig. 4. Impurity concentrations in Mg melted in SUS430 crucible at (a) 1 073 K, (b) 1 173 K, and (c) 1 273 K. (Online version in color.)

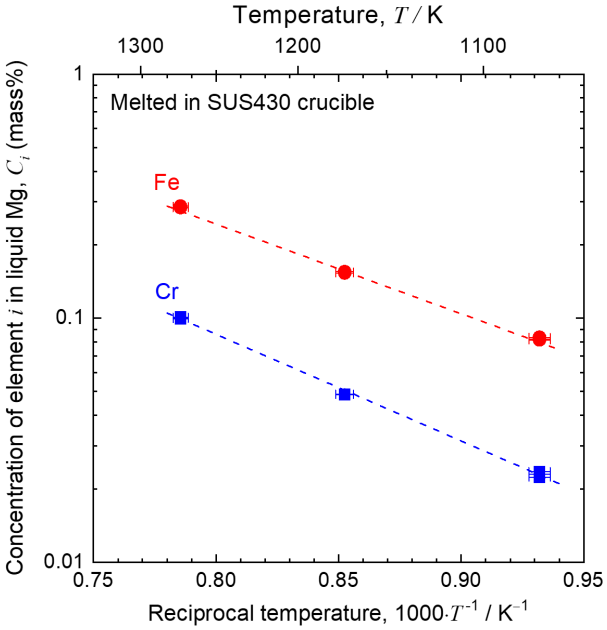

Fig. 5. Temperature dependence of Fe and Cr concentrations in Mg. (Online version in color.)

3.2. Composition Changes in Stainless Steel Surfaces

Figures 6 and **7** show the typical analytical results of the sectional interface between Mg and SUS430, and they were obtained after the melt holding process at 1 273 K for 96 h (Exp. SUS430_10) at low and high magnifications, respectively. At least in the EPMA performed in this study, no significant change was observed in the compositions of Fe and Cr in SUS430 near the interface with Mg (Figs. 6(b) and 7(b)). As listed in **Table 4**, the Cr/Fe mass ratio in Mg after the melt holding process was close to the Cr/Fe mass ratio in SUS430. The almost unchanged composition of Fe and Cr in SUS430 is reasonable in terms of their dissolution ratio in liquid Mg.

Compared with the original composition of the SUS430 crucible, Mn concentration near the inner wall of the crucible decreased due to contact with liquid Mg. When Mg was melted at 1 273 K for 96 h, Mn concentration in SUS430 was lower than the original concentration (approximately 1 mass%) over a depth of approximately 400 μm from the inner wall of the crucible; the concentration was approximately 0.8 mass% on the surface of SUS430 (Figs. 6(c) and 7(c)). The Mn/Fe mass ratio in Mg after the melt holding process was more than one order of magnitude larger than that in SUS430 (Table 4); this is consistent with the decrease in Mn concentration near the surfaces of SUS430.

As shown in Table 4, the Ni/Fe and Cr/Fe mass ratios in Mg after the melt holding process were both one order of magnitude greater than that in SUS430. Therefore, the concentrations of Ni and Cu in SUS430 was considered to decrease near the inner wall surfaces compared to the original composition. However, clear information was not obtained by the EPMA because the concentrations of Ni and Cu in SUS430 were originally low.

4. Discussion

4.1. Impurity Concentrations in Liquid Magnesium

Figure 8 shows the solubility limits of element i (Fe, Cr,

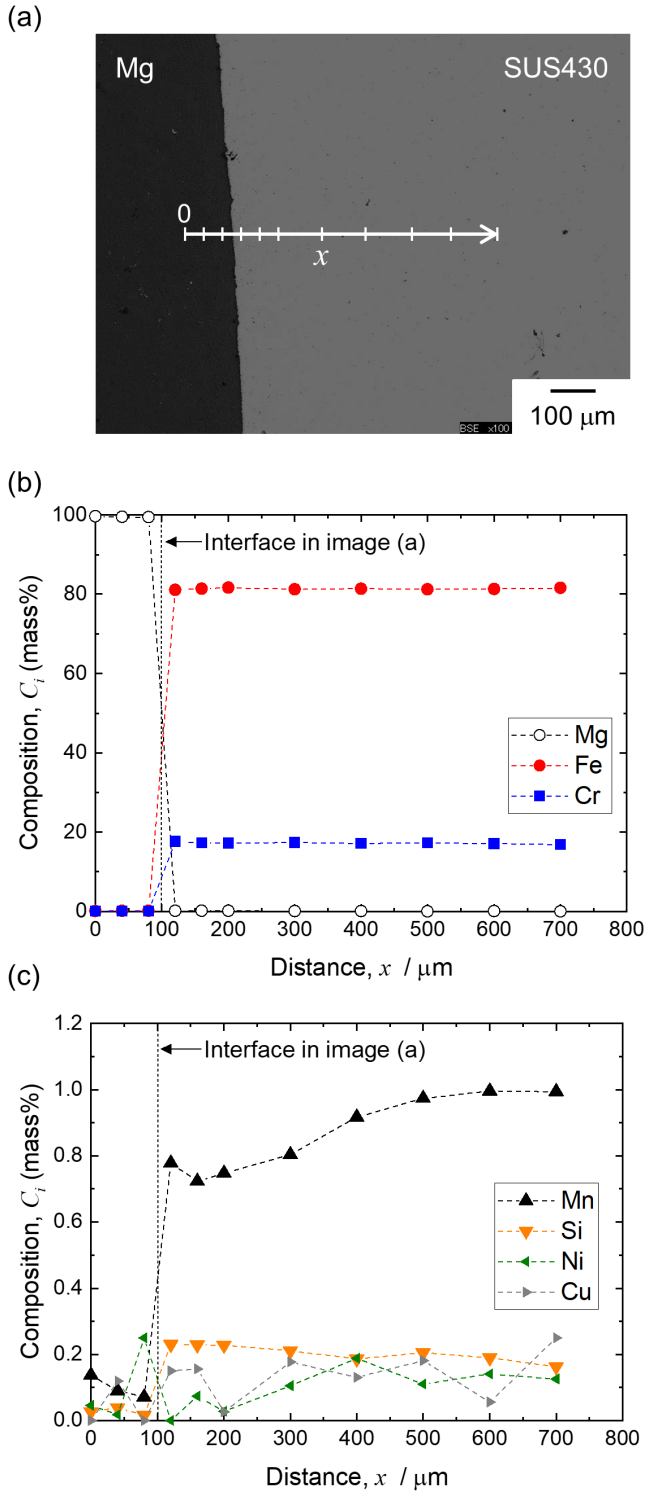

Fig. 6. (a) Backscattered electron image and (b,c) composition profiles for the interface between Mg and SUS430 crucible heated at 1 273 K for 96 h (Exp. SUS430_10). Observation results at low magnification. (Online version in color.)

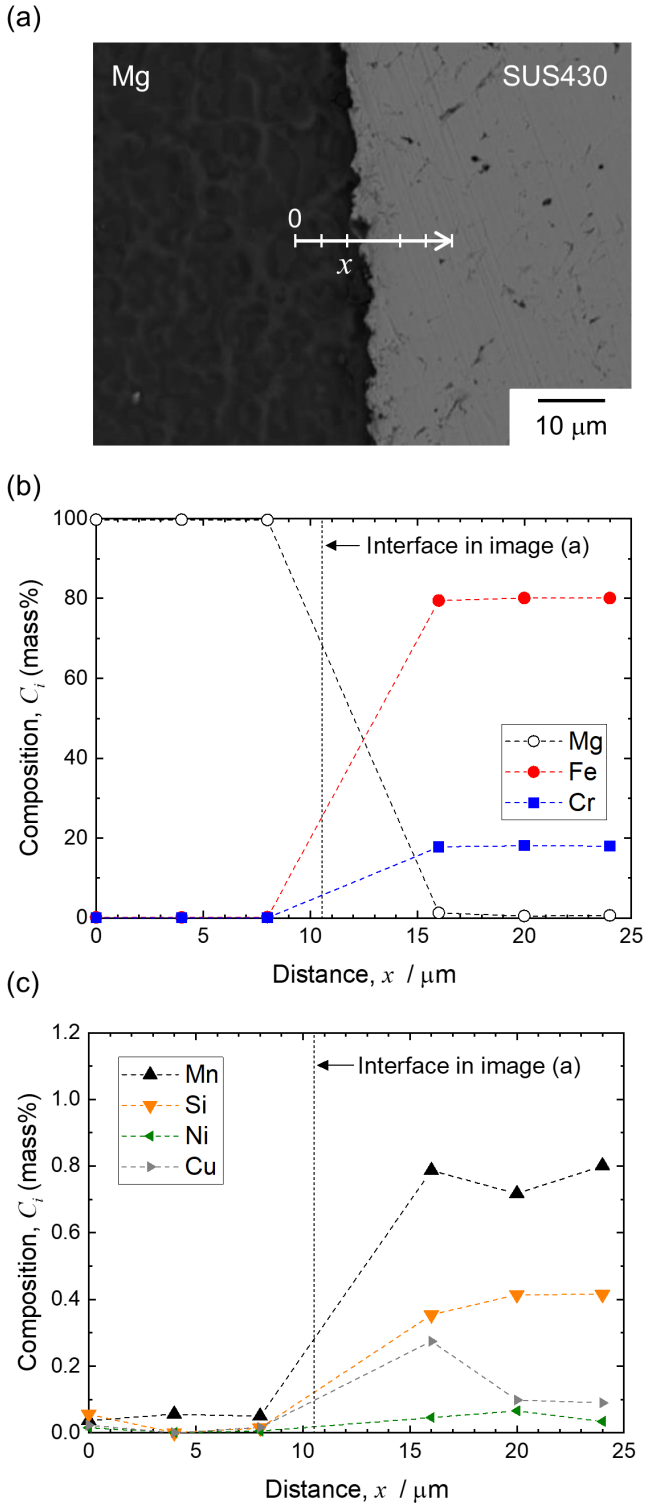

Fig. 7. (a) Backscattered electron image and (b,c) composition profiles for the interface between Mg and SUS430 crucible heated at 1 273 K for 96 h (Exp. SUS430_10). Observation results at high magnification. (Online version in color.)

Mn, Ni, and Cu) in the Mg–*i* binary systems.[9,22–24] Fe and Cr, the main components of SUS430, do not form intermetallic compounds with Mg and have low solubility limits in liquid Mg.[1,2,9,22,25] Similar to Fe and Cr, Mn does not form intermetallic compounds with Mg; however, the solubility limit of Mn in liquid Mg is approximately one order of magnitude greater than that of Fe or Cr.[23] Therefore, the dissolution of Mn was as large as that of Cr (Fig. 4) even though the Mn content in SUS430 was less than 1 mass% (Table 2). In contrast, Ni and Cu form intermetallic compounds with Mg owing to their high affinity with Mg and have high solubilities in liquid Mg in the binary systems.[23,24] Thus, Ni and Cu dissolved from SUS430 and contaminated Mg (Fig. 4) even when their concentrations in the SUS430 were as low as approximately 0.2 mass% (Table 2).

In this study, the steady-state concentrations of Fe and Cr in Mg ($C^*_{i\text{ in Mg}}$) were determined experimentally (Fig. 5, Eqs. (1) and (2)). Therefore, the authors estimated the

Table 4. Mass ratios of various impurity elements in Mg.

Exp. no.	Melt holding process		Mass ratio[a]			
	Temp., T/K	Time, t'/h	Cr/Fe	Mn/Fe	Ni/Fe	Cu/Fe
SUS430_01	1 073	24	0.28	0.18	0.052	0.040
SUS430_03		48	0.28	0.26	0.090	0.068
SUS430_06		96	0.27	0.32	0.12	0.086
SUS430_04	1 173	24	0.32	0.23	0.069	0.054
SUS430_07		48	0.31	0.27	0.10	0.077
SUS430_09		96	0.32	0.32	0.14	0.11
SUS430_05	1 273	24	0.35	0.27	0.13	0.10
SUS430_08		48	0.35	0.30	0.15	0.11
SUS430_10		96	0.35	0.38	0.23	0.18
Reference			0.20[b]	0.011[b]	0.0027[b]	0.0022[b]

a: Calculated based on the impurity composition of Mg listed in Table 3.
b: Mass ratio of SUS430 used in this study. Calculated based on the compositional data presented in Table 2.

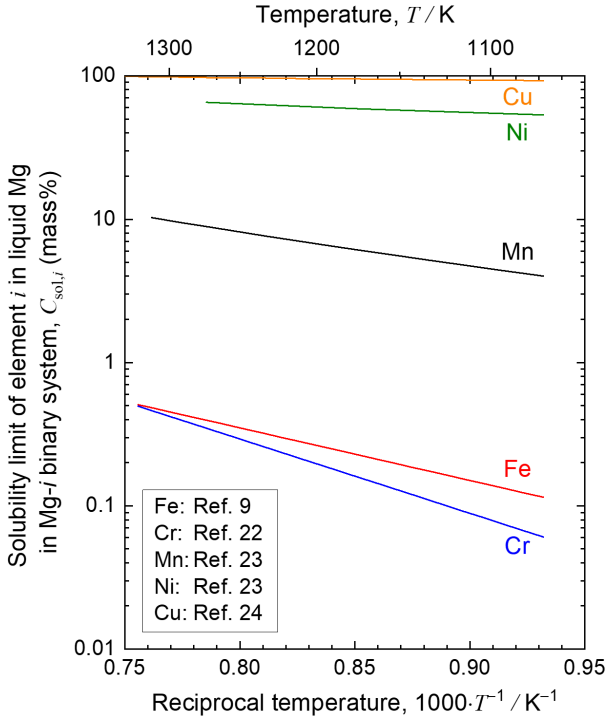

Fig. 8. Solubility limits of various elements in liquid Mg.[9,22–24] (Online version in color.)

solubility limits of Fe and Cr in liquid Mg in the presence of SUS430 based on the thermodynamic data available for SUS430 and the Mg–Fe and Mg–Cr binary systems; the estimated values were then compared with $C^*_{i\text{ in Mg}}$.

Arai and Takeda[26] formulated the activity coefficients of Fe and Cr in the ferrite phase (γ, i = Fe or Cr) based on the experimental data reported for the Fe–Cr and Fe–Cr–Ni systems as follows:

$$\gamma_{Fe} = \exp\left[\left(3\,250/T - 2.57 + 1.24X_{Cr}\right)X_{Cr}^{\,2}\right], \quad \ldots\ldots (3)$$

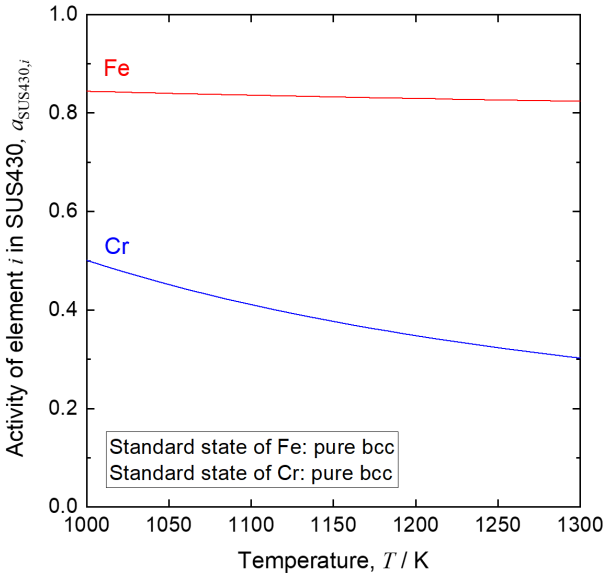

Fig. 9. Temperature dependence of assessed activities of Fe and Cr in SUS430. (Online version in color.)

$$\gamma_{Cr} = \exp\left[\left(3\,250/T - 1.95 + 1.24X_{Cr}\right)\left(1 - X_{Cr}\right)^2\right], \quad \ldots (4)$$

where X_i is the mole fraction of element i in steel. The standard states for Fe and Cr are pure bcc Fe and pure bcc Cr, respectively. Composition of the SUS430 used in this study can be approximated as $Fe_{0.82}Cr_{0.18}$ (X_{Fe} = 0.82, X_{Cr} = 0.18) from the composition shown in Table 2. Based on this approximate composition and Eqs. (3) and (4), the authors assessed the activities of Fe and Cr in the SUS430 ($a_{SUS430,i} = \gamma_i \cdot X_i$). **Figure 9** shows the temperature dependence of $a_{SUS430,i}$ evaluated in this study.

According to the available literature,[9] the solubility limit of Fe in liquid Mg in the presence of pure Fe ($C^\circ_{sol,Fe}$ (mass%)) can be expressed as follows:

$$\log\left(C^\circ_{sol,Fe}\right) = -3.67\times10^3/T + 2.48\left(\pm0.06\right) \quad [1\,073 - 1\,323\ \mathrm{K}]. \quad \ldots (5)$$

Additionally, the solubility limit of Cr in liquid Mg in the presence of pure Cr ($C^\circ_{sol,Cr}$ (mass%)) was reported to be

$$\log\left(C^\circ_{sol,Cr}\right) = -5.18\times10^3/T + 3.61\ \left(\pm0.07\right) \quad [1\,073 - 1\,323\ \mathrm{K}].^{22)} \quad \ldots (6)$$

If liquid Mg is equilibrated with solid metal i whose activity is $a_{SUS430,i}$, the solubility limit of i in liquid Mg is given by $a_{SUS430,i} \cdot C^\circ_{sol,i}$.

In **Fig. 10**, the experimentally determined values of $C^*_{i\text{ in Mg}}$ are compared with the values of $a_{SUS430,i} \cdot C^\circ_{sol,i}$, and these are in good agreement for both Fe and Cr. This result suggests the validity and reliability of the $C^*_{i\text{ in Mg}}$ determined in this study. Although Mg melted in the SUS430 crucible contained various impurities, the saturated concentrations of Fe and Cr in liquid Mg could have been determined mainly by the binary interaction with Mg (Mg–Fe and Mg–Cr interactions, respectively). Therefore, even when liquid Mg is physically contacted with steel with different Cr contents, the maximum contamination with Fe and Cr may be predicted with sufficient accuracy for practical use

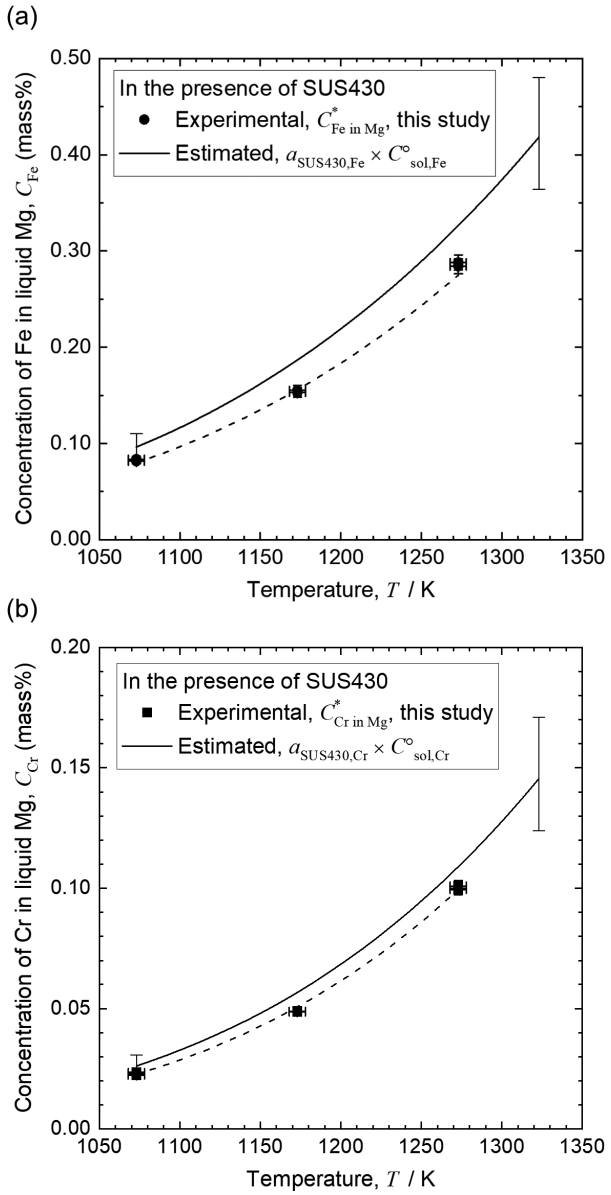

Fig. 10. Comparison of the concentration data for (a) Fe and (b) Cr in liquid Mg in the presence of SUS430.

by multiplying the assessed activity of i in steel and available $C^\circ_{sol,i}$ data.

4.2. Impurity Uptake from Liquid Magnesium in Titanium Smelting

In the current Ti smelting process known as the Kroll process, the overall reaction of the reduction step to produce Ti sponge is expressed as follows:

$$TiCl_4(l,g) + 2Mg(l) = Ti(s) + 2MgCl_2(l). \quad \text{.....(7)}$$

For producing 1 ton of Ti sponge, at least 4 tons and 1 ton of $TiCl_4$ and Mg are required, respectively. In the reduction step, Fe and other impurities dissolved in liquid Mg used as a reductant are transferred into the produced Ti sponge, thereby deteriorating its quality. In this section, the authors evaluated the impurity contamination via liquid Mg using the obtained experimental data. For simplicity, only Fe and Cr were considered as impurity elements dissolved from the steel into liquid Mg.

Figure 11 shows the Mg cycle in current typical Ti smelters. The reduction step to produce Ti sponge is a batch-type process. Liquid Mg is loaded in a gas-tight steel vessel and kept at approximately 1 073 K under Ar atmosphere. Subsequently, high-purity $TiCl_4$ is introduced into the vessel to produce Ti sponge by reaction (7). The byproduct of the Ti reduction process, $MgCl_2$, is converted into Mg metal and chlorine gas by molten salt electrolysis. The Mg metal is reused in the reduction step, while chlorine gas is used in the carbochlorination process to produce $TiCl_4$ from Ti ore.

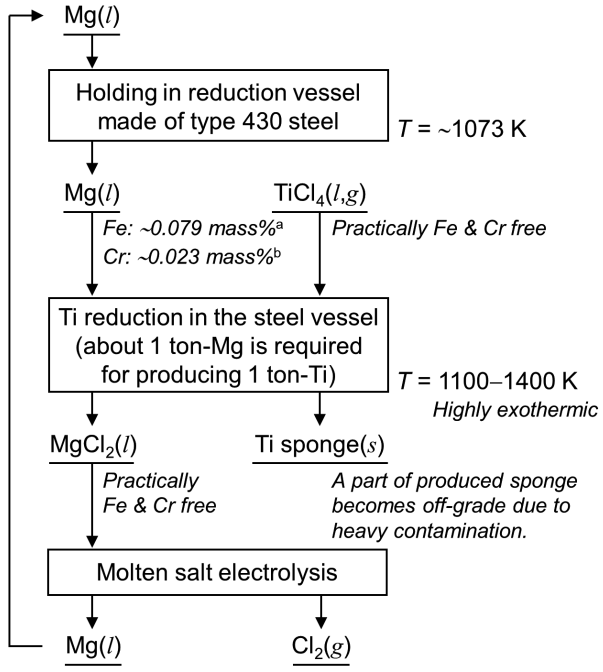

a: Calculated using Eq. (1).
b: Calculated using Eq. (2).

Fig. 11. Mg cycle in the current Ti smelting process (Kroll process). The concentrations of Fe and Cr in liquid Mg, estimated under the assumption that the reduction vessel is composed of SUS430 steel, is also shown. Note that the reduction vessel is typically composed of austenitic stainless steel or carbon-steel-lined austenitic stainless steel in practical industrial operation.

In Japanese smelters, the current batch size of the reduction vessel is approximately 10 tons. In the practical industrial operation, Mg reductant is semi-continuously charged into the reduction vessel, and the byproduct $MgCl_2$ is tapped out intermittently; the reduction vessel is often composed of austenitic stainless steel or carbon-steel-lined austenitic stainless steel. However, for simplifying the evaluation, it is assumed that 10 tons of Mg is kept at 1 073 K in a SUS430 vessel at the start of the reduction step. In this case, it is calculated using Eqs. (1) and (2) that the concentrations of Fe and Cr in liquid Mg can increase up to 0.079 ± 0.004 mass% and 0.023 ± 0.001 mass%, respectively. Thus, it can be estimated that 10 tons of Mg held in the vessel contains up to ~8 kg and ~2 kg of Fe and Cr, respectively, which are transferred into Ti as the reduction reaction (7) progresses.

During the reduction step, liquid Mg in the vessel acts as a medium for transporting Fe from the inner wall of the vessel to the Ti sponge. The reduction reaction (7) is an intense exothermic reaction. Although the vessel walls are cooled to ensure a reaction temperature below 1 173 K, the temperature inside the vessel reaches up to approximately

1 273 K depending on the position. Equation (1) indicates that the saturated concentration of Fe in liquid Mg at 1 273 K (~0.28 mass%) is approximately 1.8 times the value at 1 173 K (~0.16 mass%). Further, Eq. (2) indicates that the saturated concentration of Cr in liquid Mg at 1 273 K (~0.099 mass%) is approximately 1.9 times the value at 1 173 K (~0.051 mass%). Therefore, the impurity transport capacity of liquid Mg present in the vessel increases with an increase in temperature. It is quantitatively understood that efficiently removing the reaction heat and suppressing the temperature rise within the reduction vessel are important for reducing the contamination of the Ti sponge.

In the current industrial practices, the direct removal of Fe and other impurities from Ti is not feasible during the melting process of Ti sponge and in subsequent processes. Thus, Ti sponge with relatively high levels of impurities cannot be used as a raw material for producing ingots of Ti and its alloys. Although the extent of contamination depends on the size of the reduction vessel and operating conditions, approximately 10–20% of the produced Ti sponge becomes off-grade due to heavy contamination and is usually used in cascade as steel additives. The quantitative analysis shown in this study will help to improve the process conditions for increasing the efficiency of Ti sponge production.

5. Conclusion

The dissolution of various metallic elements (Fe, Cr, Mn, Ni, and Cu) from SUS430 ferritic stainless steel into liquid Mg was quantitatively evaluated at 1 073–1 273 K. The amount of each element dissolved in Mg was in the order of Fe > Cr ≈ Mn > Ni > Cu during the melt holding time of 24–96 h. The dissolution of each element increased with increasing temperature at a constant holding time. The concentrations of Fe and Cr in Mg reached a steady state within a holding time of 24 h, and the relationships between the concentrations ($C^*_{i\text{ in Mg}}$ (mass%), i = Fe or Cr) and temperature (T/K) are expressed as follows:

$$\log\left(C^*_{\text{Fe in Mg}}\right) = -3.68\times10^3 / T + 2.33\left(\pm0.02\right),$$

$$\log\left(C^*_{\text{Cr in Mg}}\right) = -4.37\times10^3 / T + 2.43\left(\pm0.02\right).$$

In contrast, the concentrations of Mn, Ni, and Cu in Mg increased with an increase in holding time and did not reach a steady state even after 96 h. Compared to the original composition, a decrease in Mn concentration on the inner wall of the SUS430 crucible was also confirmed.

The experimentally determined impurity concentrations in Mg were validated through discussion using thermodynamic data available for the Mg–i binary systems and SUS430. Furthermore, it was estimated that the Mg–Fe and Mg–Cr binary interactions dominated the saturated concentrations of Fe and Cr in liquid Mg, respectively, and that the influence of interactions with other dissolved elements was slight. The findings of this study provide useful fundamental information for controlling the impurity levels in melting and casting of Mg and its alloys as well as in Ti smelting using Mg as a reductant.

Acknowledgments

The authors are grateful to Messrs. Kazuhiro Taki, Masanori Yamaguchi, Yosuke Inoue of Toho Titanium Co., Ltd. for providing valuable information on Ti smelting. The authors also thank Dr. Yasushi Kato of JFE Techno-Research Corporation, Prof. Toshihiro Tsuchiyama and Dr. Takuro Masumura of Kyushu University for providing useful insights into stainless steels. The authors appreciate the help recieved from Mr. Satoshi Oue, Ms. Sachiyo Takasaki, and Prof. Shinji Munetoh of Kyushu University with the microstructure observation.

REFERENCES

1) O. Kubaschewski: Iron-Binary Phase Diagrams, Springer, Berlin, Heidelberg, (1982), 59.
2) A. A. Nayeb-Hashemi, J. B. Clark and L. J. Swartzendruber: *Bull. Alloy Phase Diagr.*, **6** (1985), 235. https://doi.org/10.1007/BF02880405
3) K. Sakakibara: *J. JFS*, **86** (2014), 639 (in Japanese). https://doi.org/10.11279/jfes.86.639
4) F. Habashi, ed.: Handbook of Extractive Metallurgy, Vol. 2, VCH Verlagsgesellschaft mbH, Weinheim, (1997), 1129.
5) H. Kusamichi, J. Iseki, A. Moriya, A. Kanai, T. Nishimura, H. Kanayama and T. Kusamichi: Titanium Industry in Japan and Its New Technologies, AGNE Gijutsu Center, Tokyo, (1996), 1 (in Japanese).
6) J. D. Hanawalt, C. E. Nelson and J. A. Peloubet: *Trans. Am. Inst. Min. Metall. Eng.*, **147** (1942), 273.
7) Magnesium Technology: Metallurgy, Design Data, Applications, eds by H. E. Friedrich and B. L. Mordike, eds, Springer, Berlin, Heidelberg, (2006), 1. https://doi.org/10.1007/3-540-30812-1
8) A. A. Nayeb-Hashemi and J. B. Clark: *Bull. Alloy Phase Diagr.*, **6** (1985), 238. https://doi.org/10.1007/BF02880406
9) Y. Taninouchi, K. Nose and T. H. Okabe: *Metall. Mater. Trans. B*, **49** (2018), 3432. https://doi.org/10.1007/s11663-018-1384-7
10) J. C. Viala, D. Pierre, F. Bosselet, M. Peronnet and J. Bouix: *Scr. Mater.*, **40** (1999), 1185. https://doi.org/10.1016/S1359-6462(99)00028-7
11) D. Pierre, F. Bosselet, M. Peronnet, J. C. Viala and J. Bouix: *Acta Mater.*, **49** (2001), 653. https://doi.org/10.1016/S1359-6454(00)00346-3
12) D. Pierre, M. Peronnet, F. Bosselet, J. C. Viala and J. Bouix: *Mater. Sci. Eng. B*, **94** (2002), 186. https://doi.org/10.1016/S0921-5107(02)00071-5
13) D. Pierre, J. C. Viala, M. Peronnet, F. Bosselet and J. Bouix: *Mater. Sci. Eng. A*, **349** (2003), 256. https://doi.org/10.1016/S0921-5093(02)00793-1
14) C. K. Tang, M.-A. Van Ende and I.-H. Jung: Magnesium Technology 2012 (Proc. TMS 2012 Annual Meeting and Exhibition), John Wiley and Sons, Hoboken, NJ, (2012), 261. https://doi.org/10.1007/978-3-319-48203-3_48
15) F. Czerwinski: Magnesium Alloys, Properties in Solid and Liquid States, IntechOpen, London, (2014), 131. https://doi.org/10.5772/59181
16) K. Kaitoh, T. Motegi and E. Satoh: *J. Jpn. Inst. Light Met.*, **45** (1995), 708 (in Japanese). https://doi.org/10.2464/jilm.45.708
17) C. Scharf and A. Ditze: *Adv. Eng. Mater.*, **9** (2007), 566. https://doi.org/10.1002/adem.200600280
18) M. Sonoda, Y. Takahashi, H. Era and N. Shinozaki: *J. JFS*, **88** (2016), 663 (in Japanese). https://doi.org/10.11279/jfes.88.663
19) T. Chen, X. Xiong, Y. Yuan, A. Tang, D. Li, A. Atrens and F. Pan: *Adv. Eng. Mater.*, **22** (2020), 2000338. https://doi.org/10.1002/adem.202000338
20) Y. Taninouchi and T. H. Okabe: *Metall. Mater. Trans. B*, **52** (2021), 611. https://doi.org/10.1007/s11663-020-02025-1
21) JIS G 4303: 2012, Stainless steel bars (in Japanese).
22) Y. Taninouchi, T. Yamaguchi, T. H. Okabe and H. Nakano: *Metall. Mater. Trans. B*, **53** (2022), 1851. https://doi.org/10.1007/s11663-022-02494-6
23) FactSage Thermochemical Software (version 7.3), FTlite database, GTT-Technologies and Thermfact Ltd., Herzogenrath and Mount Royal, QC, (2019).
24) FactSage Thermochemical Software (version 7.3), BINS database, GTT-Technologies and Thermfact Ltd., Herzogenrath and Mount Royal, QC, (2019).
25) H. Okamoto: *J. Phase Equilib.*, **21** (2000), 209. https://doi.org/10.1361/105497100770340336
26) H. Arai and S. Takeda: *Tetsu-to-Hagané*, **72** (1986), 831 (in Japanese). https://doi.org/10.2355/tetsutohagane1955.72.7_831